JOURNAL OF CHEMICAL & ENGINEERING DATA

Article

pubs.acs.org/jced

Salt-Forming Regions of Na^+, $Mg^{2+}//Cl^-$, $SO_4^{2-}-H_2O$ System at 373.15 K in the Nonequilibrium State of Isothermal Boiling Evaporation

Huan Zhou,* Jianbo Zhang, Hongli Zhang, Shuai Zhang, Xiaoqin Bai, and Zuoliang Sha

Tianjin Key Laboratory of Marine Resources and Chemistry, College of Marine Science and Engineering, Tianjin University of Science and Technology, Tianjin TEDA, 300457, P. R. China

ABSTRACT: The salt-forming regions for the complex salt−water system in the nonequilibrium state are more complex and do not always follow the solubility diagram. To understand the behaviors of the salt-forming region departing from the equilibrium phase area, the experimental investigation of the salt-forming regions in a nonequilibrium state for the quaternary system of Na^+, $Mg^{2+}//Cl^-$, $SO_4^{2-}-H_2O$ at the isothermal boiling temperature of 373 ± 0.2 K was carried out. The 32 specifically saturated solutions were evaporated with an average evaporation intensity of (1.8 to 2.4) g/(L·min)(water). Based on the liquid phase routes and solid precipitated sequence, the solid-forming regions for mainly salts were determined, respectively, where the regions of halite, thenardite, vanthoffite, and loeweite are enlarged, and they are 1.87, 1.76, 1.85, and 1.25 times bigger, respectively, than those solubility region, whereas d'ansite and kieserite regions are reduced. Furthermore the so-called *salt-forming diagram* composed of the salt-forming regions shows the stability of salt-forming regions in the nonequilibrium state, and the so-called *isothermal diagram* combined a salt-forming diagram with the solubility diagram, giving five one-salt stable regions and a complex conditional region (including eight two-salt regions and four three-salt regions). The conditional region does not exist in the solubility diagram and metastable diagram but exists in the salt-forming diagram and occupies a field about 47 % of the diagram's total area where the salt precipitating depends on nonthermodynamic conditions, such as crystal seed, evaporation intensity, mechanical effects, and so forth. Thus, knowledge of the salt-forming region, especially the conditional salt-forming region, would be extremely valuable to industry process design and control.

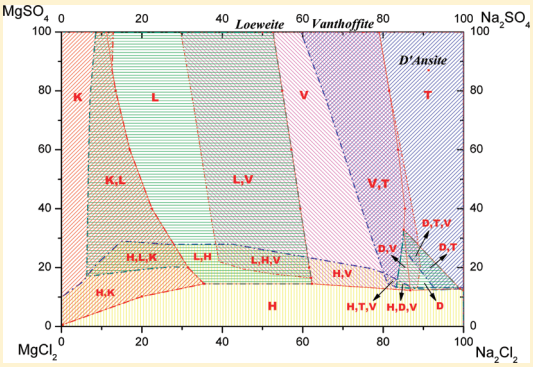

INTRODUCTION

Complex inorganic salt−water systems, such as seawater, salt lake, sea salt residual brine or bittern, or some industrial wastewaters, are salt resources. Evaporation yields a crystallization sequence of various simple salts, salt hydrates, and double salts. To recover valuable salts, spontaneous evaporation and cool crystallization under natural conditions may be considered; meanwhile, multiple-effect evaporation or mechanical refrigeration crystallization coupling with other industrial processes, such as desalination, power generation, and metallurgy, may also be adopted. Phase diagrams are thus important tools when designing fractional crystallization processes or verifying and analyzing process simulation and optimization results. However, because the metastable phenomena are typical for those complex salt−water systems and the industry processes are usually run in the nonequilibrium state where supersaturation exists, thus the salt-forming sequences are more complex, and even the salt-forming regions cannot be always accurately predicted by the solubility diagram or metastable phase diagram. Therefore, it is necessary to know more about the phenomena and behaviors of salt forming in the nonequilibrium state.

Solubility Diagram. Beginning with van't Hoff and continued by D'Ans, Autenrieth, Braitsch, Emons, and the Russian school of Kurnakov, Lepeshkov, and Zdanovskii et al., the solubility of seawater type and related systems has been studied for nearly 100 years.[1] Thereby, the methodology of isothermal solubility equilibria to determine solid−liquid equilibrium (SLE) data and the graphical representation and thermodynamic modeling of solubility equilibria in multicomponent salt−water systems have been developed and used as classical guidelines for new experiments or new process development.

Metastable Phase Diagram. Even though the number of available solubility data is large in literature, the seawater system is still under-exploited, due to the complexity of the system or the lack of reliable data in some solubility fields.[2] Moreover, metastable phenomena occur in the complex systems, so that its salt precipitation sequence does not always follow the solubility diagrams. Thereby, the metastable phase diagram determined by the isothermal evaporation method is also used to present the phase regions within natural evaporation processes, such as the so-called "solar phase diagram" of the Na^+, K^+, $Mg^{2+}//Cl^-$, $SO_4^{2-}-H_2O$ system at 298 K (partial) by Kurnakov and Nikolaev[3] and at (288, 298, and 305) K by Jin et al.[4−6] In recent years, more data about the metastable equilibria

Received: November 27, 2011
Accepted: March 2, 2012
Published: March 20, 2012

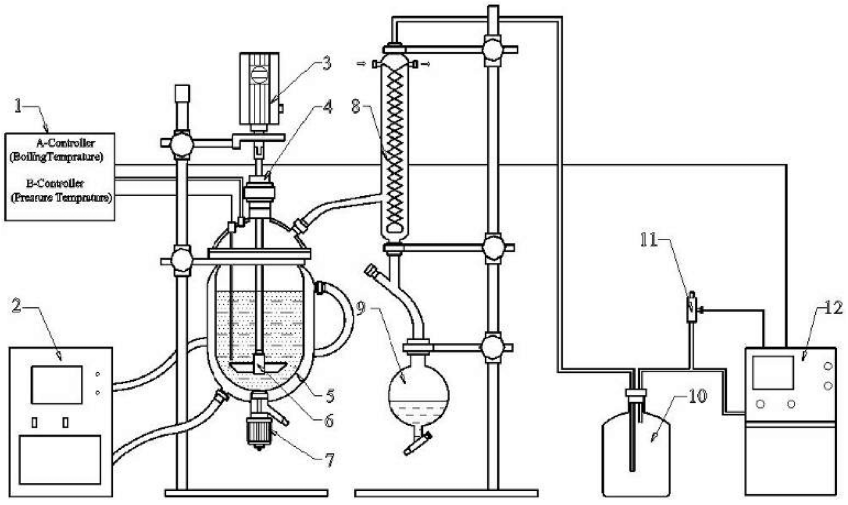

Figure 1. Experimental apparatus: 1, the controller of steam pressure and temperature; 2, thermostatic oil bath; 3, Heidolph stirrer; 4, sealed subassembly; 5, oil jacket glass reactor; 6, stirrer; 7, valve; 8, water vapor condenser; 9, water collector; 10, buffer bottle; 11, vacuum control valve; 12, vacuum pump.

of sulfate, carbonate, and borate and Li^+, Mg^{2+}, and Rd^+ containing systems at ambient temperature are published by Sang et al.,[7,8] Zeng et al.,[9,10] Deng et al.[11−13] The reasoning of metastable phenomena was also studied through crystallization kinetics with an isothermal decrease of the supersaturation method[14] or on the micromechanism of solution with Raman spectroscopy[15] by Tepavitcharova et al. The solution structure was also studied with an X-ray diffraction method by Fang et al.[16]

Salt-Forming Behavior in Nonequilibrium State. Evaporation processes such as multieffect evaporation are usually operated at the nonequilibrium stable state or dynamic state with a high evaporation intensity at a boiling temperature from (323 to 393) K. The undesirable metastable phenomena exist but actually play a valuable role in industrial processes. For example, in the salt plant of Qarun Salt Lake (Egypt, 2005), the four-effect evaporation crystallizers run safely in loeweite and kieserite solubility regions but precipitate the desired salt of NaCl.[17] However, thermodynamic data about metastable equilibria are few and occur commonly at ambient temperature. Therefore we attempt to investigate the salt-forming behaviors in the nonequilibrium state. The previous results of the Na^+, $Mg^{2+}//SO_4^{2-}-H_2O$ system at 373 K[18] and the K^+, $Mg^{2+}//SO_4^{2-}-H_2O$ system at 348 K[19] show that (1) two salts do not coprecipitate simultaneously from the costatured solution and (2) the salt-forming regions at a given temperature largely depart from those in the solubility diagram. Considering the influence of crystal seed, the maximal and minimal regions of solid-forming NaCl were determined in literature,[20] which are 2.00 and 1.56 times larger than the NaCl solubility region; thus it is possible to utilize the bittern resources at a high efficiency. We also present the salt-forming regions of the Na^+, $Mg^{2+}//Cl^-$, $SO_4^{2-}-H_2O$ system at 348.15 K in literature.[21]

In this study, we continue the experimental investigation of salt-forming regions in the nonequilibrium state for the quaternary system of Na^+, $Mg^{2+}//Cl^-$, $SO_4^{2-}-H_2O$ at the isothermal boiling temperature of 373.15 K and attempt to document more characteristics of the salt-forming region, such as the direction and degree of the salt-forming region departing from the solubility region and its stability in industry processes.

EXPERIMENT

Chemicals and Apparatus. *Chemicals.* The chemicals used were of analytical purity grade and were recrystallized several times before use. They were all obtained from the Tianjin Kermel Chemical Reagent Ltd. $MgSO_4$ (0.990 mass fraction), NaCl (0.995 mass fraction), $MgCl_2{\cdot}6H_2O$ (0.990 mass fraction), Na_2SO_4 (0.990 mass fraction), and doubly deionized water were used to prepare the synthesized solutions and chemical analysis.

Table 1. Related Salts of the System Na^+, $Mg^{2+}//SO_4^{2-}$, Cl^-−H_2O in the Equilibrium State Phase Diagram at 373.15 K

salt name	chemical formula	symbol
halte	NaCl	H
thenardite	Na_2SO_4	T
loeweite	$Na_2SO_4{\cdot}MgSO_4{\cdot}2.5H_2O$	L
vanthoffite	$3Na_2SO_4{\cdot}MgSO_4$	V
kieserite	$MgSO_4{\cdot}H_2O$	K
d'ansite	$3NaCl{\cdot}9Na_2SO_4{\cdot}MgSO_4$	D

Apparatus. Figure 1 shows the experimental apparatus. Two L-jacketed glass evaporating crystallizers (Chemglass) with a stirrer (Heidolph), water vapor condenser with a water collector, thermostatic oil heating bath (Huber, K6s-cc-NR), chemistry diaphragm pump (vacuubrand, PC 610 NT), pressure−temperature controller, and online recorder system (homemade) were used.

Experimental Procedure. *Methodology.* The salt-forming regions were experimentally determined by the method of isothermal boiling evaporation, that is, following the moving tracks of the liquid and solid composition within the well-mixed mixture in the isothermal boiling evaporation process, getting or estimating the first salt homogeneous nucleation point (limit solubility) and the second salt heterogeneous nucleation point (boundary point), and then expressing all the series of representative routine and boundary points on the solubility diagram to show the salt-forming regions and behaviors.

Isothermal Boiling Evaporation. Based on the solubility data of the Na^+, $Mg^{2+}//Cl^-$, $SO_4^{2-}-H_2O$ system at 373.15 K,[22]

dx.doi.org/10.1021/je201239s | J. Chem. Eng. Data 2012, 57, 1192−1202

Table 2. Solid and Liquid Composition in the Isothermal Evaporation Process for the A Series Representative Points

	liquid composition (Jänecke index)			pressure			liquid composition (Jänecke index)			pressure	
no.	Na_2^{2+}	SO_4^{2-}	H_2O	KP	solid[a]	no.	Na_2^{2+}	SO_4^{2-}	H_2O	KP	solid[a]
A10	100.00	12.63	765.00	101.3		A50	62.30	14.50	727.50	101.3	
A11	100.00	12.63	730.20	74.6	H[b]	A51	62.30	14.50	698.00	71.5	H[b]
A12	100.00	13.00	733.50	75.4	H	A52	62.30	14.50	688.00	71.0	H
A13	100.00	13.18	754.97	75.2	H+T[c]	A53	53.17	18.36	680.19	70.9	H
A14	100.00	12.67	739.80	74.8	T	A54	41.74	22.89	645.57	70.1	H
A15	100.00	11.92	771.71	75.2	T	A55	31.50	26.77	601.88	69.1	H
A16	100.00	12.16	774.84	78.4	H+T[c]	A56	27.15	27.85	597.93	66.7	H+L[c]
A20	93.24	12.81	755.93	101.3		A57	13.27	20.35	551.56	61.0	H+L
A21	93.24	12.81	730.00	74.1	H[a]	A60	54.00	14.50	703.21	101.3	
A22	93.01	13.23	740.21	74.6	H+D[c]	A61	54.00	14.50	688.00	70.5	H[b]
A23	91.37	13.06	789.04	76.6	D	A62	38.00	20.00	692.00	68.0	H
A24	89.14	12.78	749.17	75.0	H+D[c]	A63	19.75	26.61	579.52	64.5	H
A25	87.16	13.24	768.41	76.1	H	A64	14.97	28.24	555.30	60.5	H
A26	83.49	14.13	734.44	76.2	H	A65	9.42	26.54	512.34	57.0	H+L[c]
A30	86.62	12.27	745.89	101.3		A66	3.93	8.08	501.97	49.8	H+L+K[d]
A31	86.62	12.27	716.20	73.5	H[b]	A67	1.49	3.48	462.68	45.7	H+K
A32	85.97	12.98	724.76	73.7	H	A70	39.00	14.60	657.00	101.3	
A33	84.83	14.32	739.09	73.9	H	A71	39.00	14.60	630.00	68.4	H[b]
A34	83.06	15.65	731.47	72.8	H	A72	27.91	17.20	634.01	68.2	H
A35	80.59	17.97	712.11	72.6	H	A73	16.74	19.87	579.45	68.2	H
A36	77.09	19.66	697.62	73.2	H+V[c]	A74	8.58	20.99	530.00	65.1	H+K[c]
A37	72.16	20.33	708.49	73.7	H+V	A75	5.53	15.97	490.83	50.3	H+K
A38	65.48	21.58	683.66	75.7	H+V	A76	2.61	6.12	464.70	45.2	H+K
A40	73.04	13.80	737.33	101.3		A80	29.09	12.65	629.60	101.3	
A41	73.04	13.80	701.50	72.5	H[b]	A81	29.09	12.65	622.00	64.5	H[b]
A42	59.21	20.88	703.64	72.8	H	A82	20.84	14.01	615.06	63.9	H
A43	53.63	23.21	676.09	71.2	H	A83	8.59	16.18	504.72	53.7	H
A44	47.08	26.47	655.60	70.6	H	A84	5.25	15.12	462.56	48.4	H+K[c]
A45	42.33	27.98	638.80	67.9	H+L[c]	A85	2.01	6.01	455.07	45.8	H+K
A46	34.85	23.70	648.84	67.5	H+L	A90	20.00	10.20	590.00	101.3	
A47	24.35	20.82	632.40	65.4	H+L	A91	20.00	10.00	580.00	60.0	H[b]
A48	13.96	18.94	573.83	61.7	H+L	A92	10.00	11.00	510.00	55.0	H
A49	5.37	15.06	489.23	50.1	H+L+K[d]	A93	5.00	11.50	470.00	48.0	H
						A94	2.00	12.00	450.00	43.2	H

[a]Solid salt: H, halite (NaCl); T, thenardite (Na_2SO_4); D, d'ansite ($3NaCl{\cdot}9Na_2SO_4{\cdot}MgSO_4$); K, kieserite ($MgSO_4{\cdot}H_2O$); L, loeweite ($Na_2SO_4{\cdot}MgSO_4{\cdot}2.5H_2O$); V, vanthofite ($3Na_2SO_4{\cdot}MgSO_4$). [b]First salt-occurring point. [c]Second salt-occurring point. [d]Third salt-occurring point.

2 L of feed solution with a certain composition on the cosaturated (univariant) curve or the invariant points was prepared by the isothermal decrease of supersaturation method and were boil-evaporated at the same temperature of 373 ± 0.2 K in an oil jacketed glass tank by a heating agent with a fixed temperature difference of 40 K. During the evaporation process, the boiling temperature was kept by adjusting the evaporating pressure to avoid its movement with the changes of the mixture content. The mixture was perfectly mixed by mechanical stirring in the whole process. The water vapor was condensed by 275 K cooling water, and the evaporation intensity was about (1.8 to 2.4) g/(L·min) which was evaluated by the stage evaporation amount between two samples and its average volume of liquid phase.

Samples. Eight to nine solid−liquid mixture samples (25 mL for each sample) were taken through the bottom valve at the occurring point of the primary nucleation and the following points of further evaporation. Moreover, the evaporation amount was also recorded by weighting the condensed water. To keep the same composition content of the liquid and solid samples with those in the tank, the mixture samples were separated by the method of nonflash isothermal filtration, which includes three key points: (1) the isothermal filter is adopted in the vacuum filtration process, (2) to avoid the flash evaporation occurring, the absolute pressure of the vacuum filtration is not lower than that in the evaporation process, and (3) it is extremely necessary to take the vacuum filtration process in a short time which normally took (3 to 5) s in our experiments.

Chemical Analysis. The composition of the liquid phases was determined by chemical analysis. The Mg^{2+} and Cl^- ion concentrations were analyzed by volumetric methods and SO_4^{2-} by the gravimetric method, and the Na^+ ion was calculated by subtraction method. The Mg^{2+} ion concentration was determined by ethylenediaminetetraacetic acid (EDTA) complexometric titration at pH 10. The Cl^- ion concentration was determined by the mole method using $AgNO_3$. The composition of SO_4^{2-} ion concentration was determined using the 0.05 M $BaCl_2$ solution. The species (see Table 1) of the solid phases were approximately evaluated with the combined wet-solid-phase method, chemical analysis, or further identified

dx.doi.org/10.1021/je201239s | J. Chem. Eng. Data 2012, 57, 1192−1202

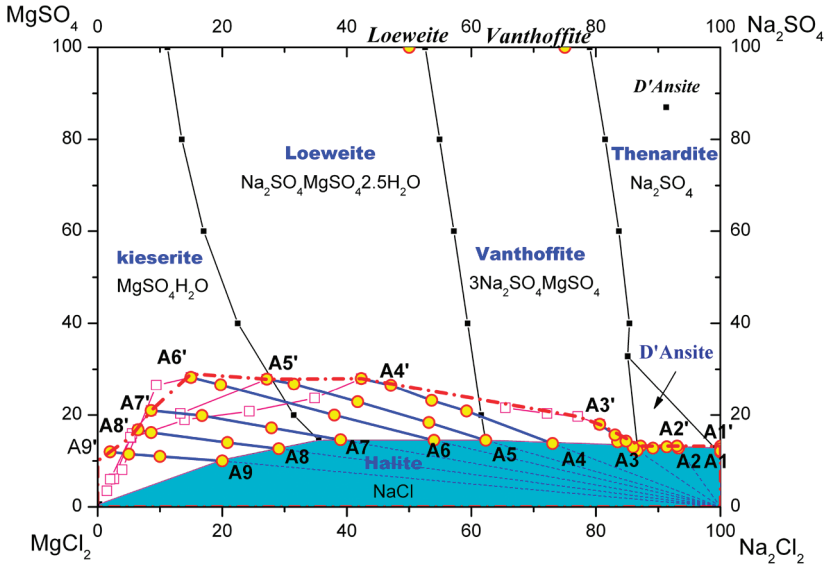

Figure 2. NaCl extended region in the Na^+, $Mg^{2+}//Cl^-$, SO_4^{2-}–H_2O system at 373.15 K in the isothermal boiling evaporation process. ■, solubility data at 373.15 K; ○, liquid phase tracks after the first salt (NaCl) forms; □, liquid phase tracks after the second salt forms; —·—, the utmost region border of solid-forming NaCl.

with XRD. The ion concentrations are expressed as the Jänecke index:

$$X_i = 100z_in_i/D \qquad Y_j = 100z_jn_j/D$$
$$Z = 100n_{H_2O}/D \qquad D = \sum z_in_i = \sum z_jn_j \qquad (1)$$

In eq 1, i and j are related to all cations and anions of the quaternary system. n and z are, respectively, the amount and the charge of a component. D is the mole number of all anions or cations, taking into account their charge to satisfy the electroneutrality condition of the medium.

RESULTS

NaCl Solid-Forming Region. The first series representative solutions (A1 to A9) cosaturated with NaCl and thenardite, d'ansite, vanthoffite, loeweite, or kieserite, respectively, were prepared and evaporated at 373 ± 0.2 K. The solid species, liquid composition, and the relevant pressure of each sample are shown in Table 2. The moving track of each representative point is presented in Figure 2.

Figure 2 shows the behaviors of solid-forming NaCl which does not completely follow the solubility diagram. Corresponding with a variation of the water content after the beginning of evaporation, the solution becomes supersaturated with sodium chloride. Then (1) NaCl and thenardite precipitate in turn for A1, and so do NaCl and d'ansite first, but NaCl precipitates singly at last for A2. (2) Only one salt of NaCl precipitates for A3 to A9 solutions; the liquid points leave the cosaturated curve and move along with the radial line of NaCl–(A3 to A9) until the second solid appears. For one representative point A6 (cosaturated with NaCl and loeweite), the liquid phase, from A6 to A6′, was concentrated to 56 %, and NaCl singly precipitating was about 89 % of the total amount in the initial feed solution.

The curve of the second salt occurring points of A1′ to A9′ gives the boundary of the NaCl solid-forming utmost field. It is the so-called salt forming region, which enlarges the NaCl scope to the adjacent fields of vanthoffite, loeweite, and kieserite to different degrees but almost keeps the same boundary with thenardite and d'ansite as those in the equilibrium state.

To illustrate the degree that the salt-forming region departs from the solubility region, the region's area was calculated by the analytical tool of calculus/integrate on the OriginPro. The total area of the diagram, for example, Figure 2, is 10 000 (100 × 100), and the area of NaCl forming region is about 2239, which is 1.87 times bigger than that in the solubility diagram (1200).

Na_2SO_4 and D'Ansite Salt-Forming Region. The second series representative solutions (B1 to B6) cosaturated with Na_2SO_4 and vanthoffite were prepared and evaporated at the fixed boiling temperature of 373 ± 0.2 K. In addition, the point B7 within the middle of Na_2SO_4 region was selected to determine the boundary of Na_2SO_4 and d'ansite. The results are shown in Table 3 and Figure 3.

Figure 3 shows that (1) Na_2SO_4 precipitates first, and the liquid phase leaves the feed point and moves along with the radial lines of Na_2SO_4–(B1 to B7) until it reaches a turning point where the second salt vanthoffite for B1 to B5, NaCl for B6, and d'ansite for B7 occurs. For example, the liquid phase of B2 moves from B2 to B2′; it is concentrated to 50.3 %, and Na_2SO_4 singly precipitating is about 54.4 % of the total amount in the initial feed solution.

(2) While the second solid phase occurs for the series experiments of B1 to B5, respectively, at the turning points (B1′, B2′, B3′, B4′, B5′), the liquid moving tracks change their direction, but the species of the second solid phase cannot be determined by vector analysis. For example, B2′ in Figure 3 does not follow the vectors of α (thenardite) or β (vanthoffite) but seemingly follows χ (loeweite); however, the XRD shows thenardite and vanthoffite were retained, but there was no loeweite in the final solid. In addition, the final solid–liquid vectors (e.g., δ for B2 feed solution) seemingly correspond to the theoretical analysis results in the equilibrium solubility diagram; that is to say, the liquid phase B2 theoretically moves along with the cosaturated curve to the final liquid point. However, the actual process in the nonequilibrium state takes a very different way where the thenardite precipitates first, and

dx.doi.org/10.1021/je201239s | J. Chem. Eng. Data 2012, 57, 1192–1202

Table 3. Solid and Liquid Composition in the Isothermal Evaporation Process for the B Series Representative Points

	liquid composition (Jänecke index)			pressure			liquid composition (Jänecke index)			pressure	
no.	Na_2^{2+}	SO_4^{2-}	H_2O	KP	solid[a]	no.	Na_2^{2+}	SO_4^{2-}	H_2O	KP	solid[a]
B10	80.39	100.00	745.53	101.3		B44	78.71	50.91	770.80	82.1	T
B11	80.39	100.00	694.00	86.4	T[b]	B45	76.76	46.29	754.03	81.8	T
B12	77.80	100.00	697.25	86.6	T	B46	74.46	40.90	731.94	80.3	T+V[c]
B13	75.92	100.00	700.72	86.7	T	B47	82.37	29.25	767.31	79.5	V
B14	70.98	100.00	669.73	86.7	T	B48	89.18	20.19	750.57	77.5	V
B15	67.86	100.00	648.62	86.6	T	B49	90.69	16.28	733.94	74.2	V
B16	63.67	100.00	629.56	86.5	T	B50	84.77	50.29	866.30	101.3	
B17	59.55	100.00	609.85	85.6	T+V[c]	B51	84.77	50.29	828.00	85.5	T[b]
B18	68.63	100.00	675.52	86.7	V	B52	83.97	46.80	838.03	86.2	T
B19	73.95	100.00	712.93	90.1	V	B53	82.19	40.68	813.12	79.2	T
B20	81.70	87.47	805.00	101.3		B54	79.83	34.33	796.84	76.3	T
B21	81.70	87.47	748.00	84.0	T[b]	B55	79.69	26.68	837.72	74.4	T+V[c]
B22	79.78	86.71	750.71	84.2	T	B56	87.82	16.39	787.48	71.9	V
B23	76.29	84.27	753.03	84.7	T	B57	88.55	13.43	794.35	71.7	V
B24	74.05	82.45	739.69	84.5	T	B58	86.13	13.34	800.75	72.0	V
B25	71.07	80.42	723.87	83.9	T	B59	83.28	13.33	737.57	72.5	V
B26	67.05	77.72	701.79	83.5	T+V[c]	B60	84.69	33.65	841.76	101.3	
B27	70.58	71.70	742.34	83.3	V	B61	84.69	33.65	805.56	740.0	T+D[c]
B28	79.55	64.56	820.10	86.8	V	B62	84.41	32.56	760.47	728.0	T+D
B29	85.04	55.72	900.13	89.8	V	B63	83.51	26.50	781.15	723.4	T+D
B30	82.55	75.35	832.50	101.3		B64	82.49	21.09	755.02	715.8	T+D
B31	82.55	75.35	752.00	84.0	T[b]	B65	81.55	16.38	768.45	702.4	T+D+H[d]
B32	81.55	73.94	755.00	84.5	T	B66	81.04	14.63	732.31	686.6	H
B33	78.75	69.96	794.13	83.6	T	B67	78.39	15.27	722.57	686.4	H
B34	75.87	65.80	780.06	82.8	T	B68	75.04	16.10	714.47	686.4	H
B35	72.82	61.07	753.00	81.7	T	B70	92.47	50.50	890.50	101.3	
B36	74.10	55.32	833.44	82.2	T+V[c]	B71	92.47	50.50	863.00	81.2	T[b]
B37	83.43	41.31	821.63	85.1	V	B72	92.22	47.66	866.53	81.9	T
B38	88.36	31.98	787.69	90.2	V	B73	91.12	42.49	872.48	81.7	T
B39	92.02	18.25	802.86	93.9	V	B74	90.38	37.25	855.64	81.7	T
B40	83.83	62.99	845.00	101.3		B75	89.72	31.31	833.29	79.9	T
B41	83.83	62.99	750.00	83.2	T[b]	B76	89.09	25.03	795.51	77.5	T+D[c]
B42	82.84	60.76	758.25	83.9	T	B77	89.15	18.94	759.86	75.7	D
B43	80.54	55.42	789.50	83.3	T	B78	93.04	12.50	760.89	74.5	D+H[d]

[a]Solid salt: T, thenardite (Na_2SO_4); V, vanthoffite ($3Na_2SO_4{\cdot}MgSO_4$); H, halite (NaCl); D, d'ansite ($3NaCl{\cdot}9Na_2SO_4{\cdot}MgSO_4$). [b]First salt-occurring point. [c]Second salt-occurring point. [d]Third salt-occurring point.

while the second solid of vanthoffite starts to precipitate, the thenardite stops its precipitating and starts to dissolve.

(3) The curve of the second salt-occurring points of B1′ to B7′ gives the boundary of Na_2SO_4-forming region which expands to vanthoffite and d'ansite solubility fields and has an area about 2555 which is 1.76 times of 1447 for the Na_2SO_4 solubility region in the solubility diagram.

Vanthoffite Salt-Forming Region. The evaporation data for the third series representative solutiond of C1 to C6 are shown in Table 4 and Figure 4.

Figure 4 shows the result of the vanthoffite-forming region. The single salt of vanthoffite forms at the first stage of evaporation; while the second salt appears, the liquid phase points are far away from the cosaturated curve of vanthoffite and loeweite. While the second salt loeweite occurs for C1 to C3, the first solid salt stops precipitating and starts dissolving. But while the second salt NaCl for C4 to C6 occurs, vanthoffit could coprecipitate, and the liquid phase does not move to the cosaturated curve of NaCl and vanthoffite. On another side of the vanthoffite region, the data of B2 to B5 evaporation show that the vanthoffite-forming region could expand to the Na_2SO_4 solubility region only while enough vanthoffite solid existed.

Vanthoffite largely expands its solid-forming scope to the loeweite solubility field, but its phase region is also occupied by NaCl. The total area of vanthoffite region is 2247 in the equilibrium state, but its salt-forming region is 4160.

Loeweite and Kieserite Region. The fourth and fifth series feed solutions of D1 to D8 and E1 to E2 were evaporated to know the features of loeweite and kieserite solid-forming regions, where D1 to D7 are very close to the cosaturated curve of loeweite and kieserite, and D8 and E1-E2 are located in the middle of loeweite and kieserite solubility regions, respectively. The results are shown in Tables 5 and 6 and Figures 5 and 6.

Figure 5 shows that the first salt precipitated for the cosaturated solutions of D1 to D7 was loeweite, and while the second salt nucleation (which is kieserite for D1 to D6 and is NaCl for D7) occurs, the liquid phases were far away from the cosaturated curve and located in the kieserite solubility region. While the second salt formed, the first salt of loeweite could coprecipitate with kieserite for D1 to D6 and with NaCl for D7 to D8. Moreover, the third salt of NaCl and kieserite come out

dx.doi.org/10.1021/je201239s | J. Chem. Eng. Data 2012, 57, 1192−1202

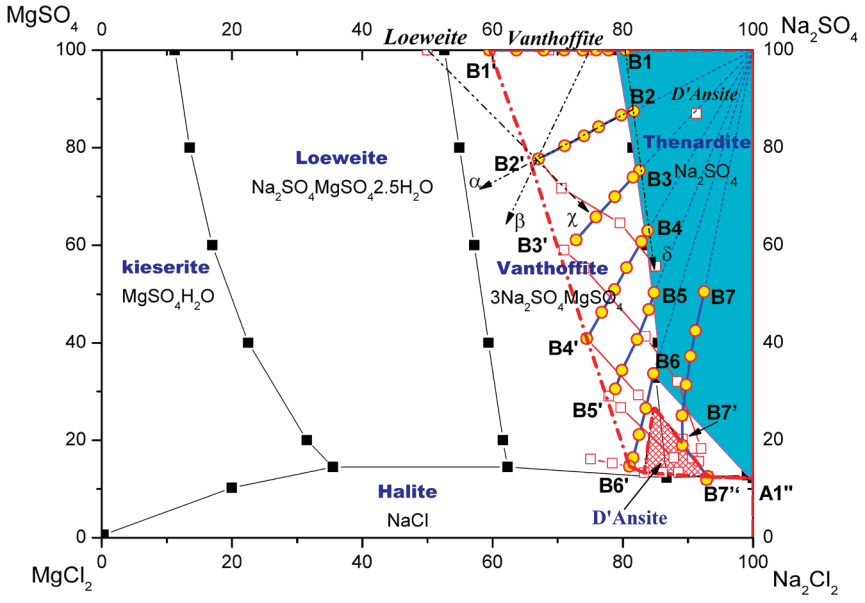

Figure 3. Na_2SO_4 extended region in the Na^+, $Mg^{2+}//Cl^-$, SO_4^{2-}–H_2O system at 373.15 K in the isothermal boiling evaporation process. ■, solubility data at 373.15 K; ○, liquid phase tracks while the first salt (Na_2SO_4) forms; □, liquid phase tracks while the second salt forms; —·—, the utmost region border of solid-forming Na_2SO_4.

Table 4. Solid and Liquid Composition in the Isothermal Evaporation Process for the C Series Representative Points

	liquid composition (Jänecke index)			pressure			liquid composition (Jänecke index)			pressure	
no.	Na_2^{2+}	SO_4^{2-}	H_2O	KP	solid[a]	no.	Na_2^{2+}	SO_4^{2-}	H_2O	KP	solid[a]
C10	51.10	100.00	725.00	101.3		C40	58.18	62.46	725.00	101.3	
C11	51.10	100.00	625.00	81.6	V[b]	C41	58.18	62.46	625.00	78.5	V[b]
C13	41.49	100.00	596.06	83.2	V	C43	54.03	53.14	699.15	78.2	V
C14	37.30	100.00	576.92	84.1	V	C44	50.32	44.97	710.91	76.9	V
C15	31.59	100.00	558.60	86.4	V	C45	46.95	37.73	697.24	74.7	V
C16	29.65	100.00	560.74	91.2	V+L[c]	C46	42.52	28.73	663.59	71.1	V+L[c]
C17	32.34	100.00	598.94	91.6	L	C47	36.64	22.25	649.74	66.5	V+H[d]
C18	37.85	100.00	693.61	91.6	L	C48	31.00	22.91	637.17	68.0	H
C20	56.09	87.38	725.00	101.3		C50	59.58	50.69	726.00	101.3	
C21	56.09	87.38	648.00	82.5	V[b]	C51	59.58	50.69	712.26	93.0	V[b]
C23	50.45	84.22	649.53	82.8	V	C53	57.34	42.40	728.64	79.0	V
C24	47.25	81.93	657.84	83.7	V	C54	53.92	32.63	729.93	74.0	V
C25	43.41	79.93	660.42	82.3	V	C55	51.48	25.02	696.40	70.1	V
C26	39.52	77.38	672.13	82.0	V	C56	46.16	20.56	748.61	67.6	V+H[c]
C27	35.17	73.82	645.36	80.7	V+L[c]	C57	36.76	21.90	643.57	66.9	V+H
C28	36.12	63.69	678.29	80.4	L	C58	26.32	25.03	631.23	64.0	V+H
C29	46.52	48.80	727.75	80.9	L	C60	72.05	50.65	779.40	101.3	
C30	56.16	74.91	725.00	101.3		C61	72.05	50.65	708.00	88.0	V[b]
C31	56.16	74.91	630.00	80.0	V[b]	C62	71.45	50.63	708.63	88.2	V
C33	50.98	67.08	691.00	80.9	V	C64	70.80	28.41	772.02	79.6	V
C34	46.53	61.35	697.70	79.9	V	C65	70.23	20.51	793.28	75.9	V
C35	42.99	56.00	687.26	78.1	V	C66	67.01	16.01	713.20	73.1	V+H[c]
C36	37.81	46.06	688.86	74.9	V+L[c]	C67	60.44	16.70	704.73	72.1	V+H
C37	37.53	34.33	691.82	73.5	L	C68	52.61	17.82	738.73	73.7	V+H
C38	39.38	21.18	656.61	73.0	L	C69	45.29	19.47	673.08	77.5	V+H
C39	39.26	20.01	661.91	81.8	L						

[a]Solid salt: L, loeweite (Na_2SO_4·$MgSO_4$·2.5H_2O); V, vanthofite ($3Na_2SO_4$·$MgSO_4$); H, halite (NaCl). [b]First salt-occurring point. [c]Second salt-occurring point. [d]Third salt-occurring point.

respectively for D4 to D6 and for D7 to D8. It is also worth noting that the liquid phase for D7, D8, and C5, respectively, did not reach the cosaturated curve of NaCl and loeweite even though loeweite precipitated first. Figure 6 shows the liquid moving tracks for E1 and E2 which did not reach the cosaturated curve even though kieserite precipitated first.

The loeweite salt-forming region is enlarged to the kieserite field and decreased by the NaCl scope. Thus, the loeweite salt-

dx.doi.org/10.1021/je201239s | J. Chem. Eng. Data 2012, 57, 1192–1202

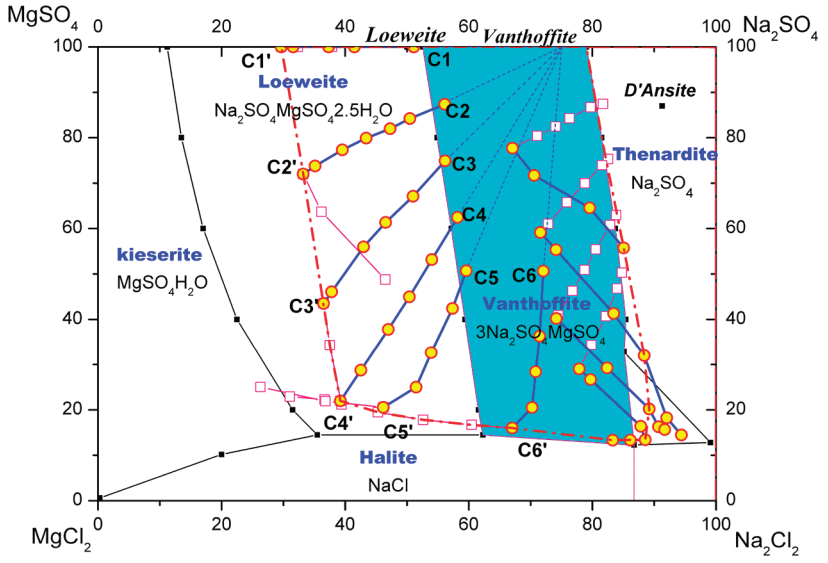

Figure 4. Vanthoffite-extended region in the Na^+, $Mg^{2+}//Cl^-$, $SO_4^{2-}-H_2O$ system at 373.15 K in the isothermal boiling evaporation process. ■, solubility data at 373.15 K; ○, liquid phase tracks while vanthoffite forms; □, liquid phase tracks while the second salt forms; —·—, the utmost region border of vanthoffite formation.

Table 5. Solid and Liquid Composition in the Isothermal Evaporation Process for the D Series Representative Points

	liquid composition (Jänecke index)			pressure			liquid composition (Jänecke index)			pressure	
no.	Na_2^{2+}	SO_4^{2-}	H_2O	KP	solid[a]	no.	Na_2^{2+}	SO_4^{2-}	H_2O	KP	solid[a]
D10	12.06	100.00	580.00	101.3							
D11	12.06	100.00	482.00	78.0	L[b]	D53	12.14	40.60	547.67	62.9	L
D12	10.12	100.00	497.50	79.7	L+K[c]	D54	8.36	35.40	510.94	65.1	L
D13	12.23	100.00	449.28	77.7	K	D55	7.50	23.90	526.00	58.5	L+K[c]
D14	12.87	100.00	425.49	74.3	K+L[c]	D56	6.13	13.30	535.60	58.0	K
D15	11.43	100.00	408.99	72.7	L	D57	4.65	8.77	532.62	52.7	K+H[d]
D16	10.60	100.00	439.40	75.1	L	D58	2.90	5.15	484.90	49.0	K+H
D17	8.53	100.00	476.23	86.1	L	D60	20.14	46.75	624.00	64.0	
D20	13.42	81.95	597.60	101.3		D61	20.14	46.75	519.97	62.5	L[b]
D21	13.42	81.95	470.00	72.0	L[b]	D62	13.63	36.95	544.87	63.0	L
D22	10.24	80.12	470.43	71.0	L	D63	10.83	30.92	525.63	58.9	L
D23	8.43	75.94	482.95	69.0	L+K[c]	D64	6.78	22.08	509.13	57.8	L+K[c]
D24	8.60	71.63	489.86	70.3	K	D65	1.46	13.88	517.51	55.7	L+K
D25	11.15	60.20	622.06	73.5	K+L[c]	D66	2.44	8.46	519.57	49.8	K+H[d]
D26	13.50	47.25	607.94	73.1	K	D67	2.08	4.34	482.66	43.9	K+H
D30	16.85	66.52	606.30			D70	24.95	37.49	635.00	101.3	
D31	16.85	66.52	489.40	68.0	L[b]	D71	24.95	37.49	604.52	64.2	L[b]
D32	12.95	61.34	494.03	67.6	L	D72	21.85	29.61	604.32	61.9	L
D33	7.40	55.50	493.24	63.1	L+K[c]	D73	20.10	24.74	552.25	61.3	L
D34	8.57	43.69	544.03	64.3	K	D74	18.2	21	551.05	60.3	L
D35	11.67	25.40	602.91	64.7	K	D75	13.60	20.64	541.98	58.7	L+H[c]
D36	12.50	14.01	594.54	64.3	K+H[d]	D76	8.50	19.08	483.20	54.8	L+H+K[d]
D40	18.60	56.61	615.00	101.3		D77	5.14	7.83	459.82	48.0	K+H
D41	18.60	56.61	523.00	64.5	L[b]	D80	36.65	50.56	681.00	101.3	
D42	10.86	45.44	532.48	64.1	L	D81	36.70	50.60	616.50	73.0	L[b]
D43	8.09	39.77	511.29	59.8	L+K[c]	D82	36.37	46.98	619.76	73.1	L
D44	10.72	22.81	532.44	58.2	K	D83	33.35	34.97	651.38	75.5	L+H[c]
D45	5.73	9.73	562.38	53.5	K+H[d]	D84	31.20	27.14	646.69	71.8	L+H
D46	3.85	5.24	476.87	50.5	K+H	D85	27.74	20.26	660.22	69.4	L+H
D50	20.37	53.93	625.00	101.3		D86	20.83	18.84	621.00	64.3	L+H
D51	20.37	53.93	575.00	65.0	L[b]	D87	13.12	18.05	612.81	59.5	L+H+K[d]
D52	18.01	49.27	597.19	65.1	L	D88	4.51	15.34	493.71	57.9	K+H

[a]Solid salt: L, loeweite ($Na_2SO_4 \cdot MgSO_4 \cdot 2.5H_2O$); K, kieserite ($MgSO_4 \cdot H_2O$);, H, halite (NaCl). [b]First salt-occurring point. [c]Second salt-occurring point. [d]Third salt-occurring point.

dx.doi.org/10.1021/je201239s | J. Chem. Eng. Data 2012, 57, 1192–1202

Table 6. Solid and Liquid Composition in the Isothermal Evaporation Process for the E Series Representative Points

	liquid composition (Jänecke index)			pressure			liquid composition (Jänecke index)			pressure	
no.	Na_2^{2+}	SO_4^{2-}	H_2O	KP	solid[a]	no.	Na_2^{2+}	SO_4^{2-}	H_2O	KP	solid[a]
E10	10.15	60.67	598.00	101.3		E17	8.57	9.15	567.58	56.5	K+H
E11	10.15	60.67	450.00	64.0	K+L[c]	E20	9.00	87.00	759.23	101.3	
E12	10.27	57.12	474.87	61.5	K+L	E21	9.00	87.00	460.58	73.5	K[b]
E13	11.05	45.66	536.45	63.9	K+L	E22	10.79	83.58	458.71	70.7	K
E14	12.79	32.83	584.25	64.5	K+L	E23	12.16	80.76	453.63	70.1	K+L[c]
E15	14.20	22.51	589.72	63.0	K+L	E24	7.99	77.48	488.23	71.0	K+L
E16	13.96	14.91	584.35	60.7	K+L+H[d]	E25	10.32	69.43	586.87	77.1	L

[a]Solid salt: L, loeweite ($Na_2SO_4 \cdot MgSO_4 \cdot 2.5H_2O$); K, kieserite ($MgSO_4 \cdot H_2O$); H, halite (NaCl). [b]First salt-occurring point. [c]Second salt-occurring point. [d]Third salt-occurring point.

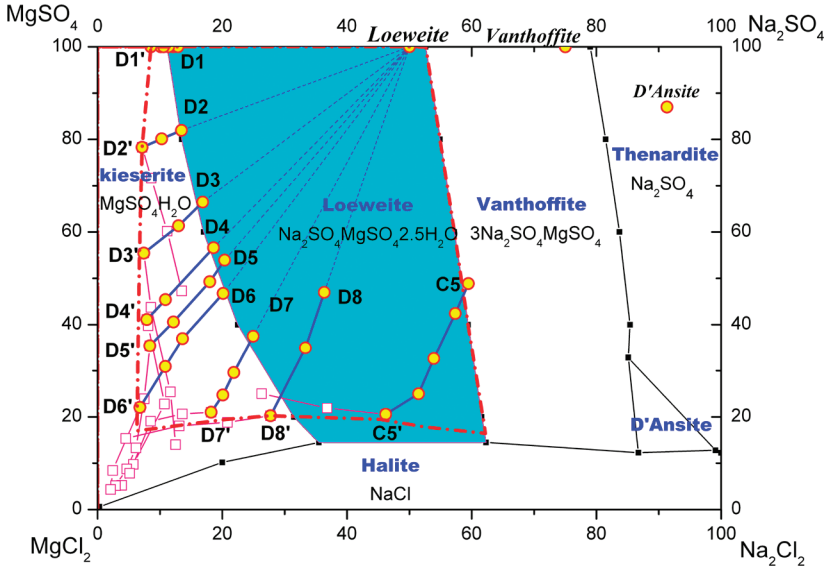

Figure 5. Loeweite solid-forming region in the Na^+, $Mg^{2+}//Cl^-$, $SO_4^{2-}-H_2O$ system at 373.15 K in the isothermal boiling evaporation process. ■, solubility data at 373.15 K; ○, liquid phase tracks while loeweite forms; □, liquid phase tracks while the second salt forms; —·—, the utmost region border of loeweite formation.

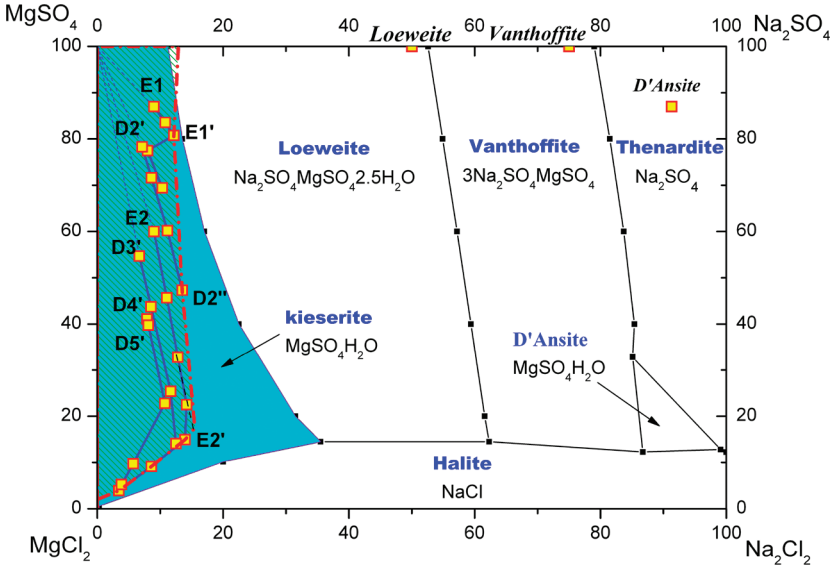

Figure 6. Kieserite solid-forming region in the Na^+, $Mg^{2+}//Cl^-$, $SO_4^{2-}-H_2O$ system at 373.15 K in the isothermal boiling evaporation process. ■, solubility data at 373.15 K; ○, liquid phase tracks while loeweite forms; □, liquid phase tracks while the second salt forms; —·—, the minimal region border of kieserite formation.

dx.doi.org/10.1021/je201239s | J. Chem. Eng. Data 2012, 57, 1192–1202

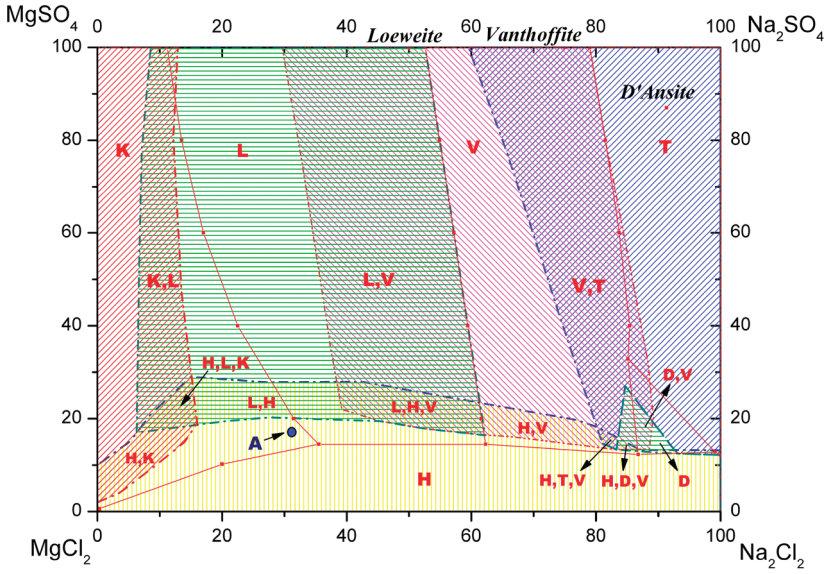

Figure 7. Isothermal salt-forming diagram of the Na^+, $Mg^{2+}//Cl^-$, SO_4^{2-}–H_2O system at 373.15 K in the nonequilibrium state. ■, solubility data at 373.15 K; –·–, border for the extended salt-forming region. D, K, L, V, T, and H denote the single salt region for d'ansite, kieserite, loeweite, vanthoffite, thenardite, and halite. K+L, L+V, V+T, L+H, H+V, H+K, and D+T denote that the region may be one or another or both. H+L+K, H+L +V, and H+D+V denote that the region may be one, two, or three salts formed in different conditions.

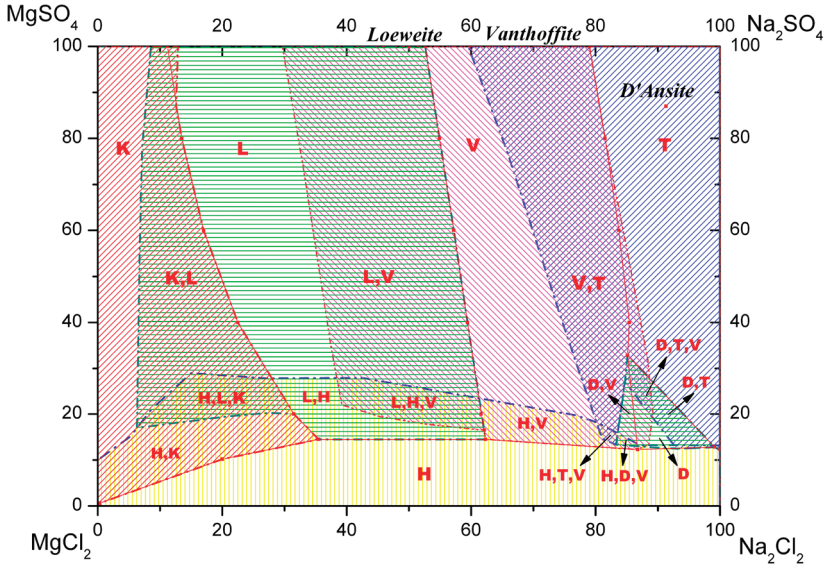

Figure 8. Isothermal diagram of the Na^+, $Mg^{2+}//Cl^-$, SO_4^{2-}–H_2O system at 373.15 K made up by the salt-forming region and solubility region. ■, solubility data at 348.15 K; –·–, border for the salt-forming region. D, K, L, V, T, and H denote the single salt region for d'ansite, kieserite, loeweite, vanthoffite, thenardite, and halite. K+L, L+V, V+T, L+H, H+V, H+K, and D+T denote that the region may be one or another or both. H+L+K, H+L +V, and H+D+V denote that the region may be one, two, or three salts formed in different conditions.

forming region has an area of about 4059, which is 1.25 times bigger than 3241 for its solubility region. By contrast, the kieserite solubility region is easy to be occupied by loeweite and NaCl, and its one salt region is reduced from 1888 to 645.

■ DISCUSSION

Mechanism of Salt-Forming Region on Crystallization Kinetics. Theoretically, it is impossible that the salt-forming region of loeweite or kieserite is occupied by NaCl in its own solubility region when its solid phase exists at first. However, in our experimental conditions, the actual results shown in Figures 4, 5, and 6 tell us that, although the loeweite or kieserite phases exist at first in its own solubility field (e.g., the points D8′, E2′), the primary nucleation of NaCl also occurs. The prior results of ref 18 and 19 show that, during the same evaporation conditions, the different salts keep a different degree of supersaturation. In this work, we noticed that, at the same evaporation intensity, the SL mixture kept a higher degree of supersaturation for loeweite or kieserite but kept a lower degree for NaCl. Thus while the solutions D8′ or E2′ are supersaturated for loeweite or kieserite at a high degree, the contents of Na^+ and Cl^- simultaneously fit to the nucleation condition of NaCl. Therefore, the coprecipitate paths in nonequilibrium state are not the same with the cosaturated curves in solubility equilibria.

Salt-Forming Diagram and Conditional Region. To know more about the characteristics of salt-forming behaviors

dx.doi.org/10.1021/je201239s | J. Chem. Eng. Data 2012, 57, 1192–1202

in nonequilibrium state, we presented all salt-forming regions in Figures 2 to 6 together on the solubility diagram and obtained the so-called salt-forming diagram.

(1) Figure 7 gives expression to six one-salt regions (K, L, V, T, H, D) and a complex intermediate zone, the overlap field, where the univariant curves in solubility diagram become two-salt intermediate zones (K+L, L+V, V+T, V+D, H+V, H+L, H +K), and the invariant points turn into three-salt intermediate zones (H+L+K, H+L+V, H+D+V, D+V+T).

(2) The species of the forming salt in the interlaced zones may be one or another or both which depends on the crystal seed species and operation conditions. Thus the conditional region was named which takes the total area of about 4028 (accounts for 40.28 % of the diagram's total area), whereas the one-salt regions, named the nonequilibrium stable region, only account for 59.72 %. Here the nonequilibrium stable-region means where the appointed salt solid phase could form whether in primary nucleation or in crystal growth, but other salts could not form in our experimental conditions.

In addition the salt-forming diagram, Figure 7, gives some information about the stability of salt-forming regions in a nonequilibrium state; for example, the "A" region is metastable for NaCl in the equilibrium state but would be stable in the nonequilibrium state.

Isothermal Diagram and Application. One salt could stably exist in its solubility region and could be formed in the salt-forming region. Combing these two regions, we obtained the most comprehensive field for one appointed salt. This field at one isothermal temperature was named the isothermal region. Figure 8 shows all of the main salts' isothermal regions, or what we call the isothermal diagram, which include five one-salt (K, L, T, D, H) stable regions and a complex isothermal conditional region. The isothermal conditional region in Figure 8 accounts for 47.06 % of the diagram's total area, which is composed of eight two-salt intermediate zones (K+H, L+V, V +T, H+K, H+L, H+V, D+V, D+T) and four three-salt intermediate zones (H+L+K, H+L+V, D+T+V, H+D+V), where the kind of salt formed depends on the non-thermodynamic conditions, such as the crystal seed species and amount, evaporation rate, stirring, and so forth.

The information about the conditional region cannot be presented by a solubility diagram or metastable diagram (because of the phase rule) but would be extremely valuable to industry process design and control, such as the utilization of bittern resources at high efficiencies.[20]

CONCLUSION

Salt-forming behaviors for the quaternary system of Na^+, Mg^{2+}// Cl^-, SO_4^{2-}−H_2O at 373.15 K by isothermal boiling evaporation were experimentally carried out with an evaporation intensity of about (1.8 of 2.4) g/(L·min), and the results were presented on a solubility diagram. The salt-forming behaviors and the characteristics of salt-forming region are summarized as follows.

(1) The salt-forming regions largely depart from those in the solubility region to different degrees. The salt-forming region for the solid phases of NaCl, Na_2SO_4, vanthoffite, and loeweite, are 1.87, 1.76, 1.85, and 1.25 times bigger, respectively, than those in the solubility diagram, but the kieserite region is reduced from 1888 in the solubility diagram to 645 in the salt-forming diagram.

(2) The so-called salt-forming diagram composed of the salt-forming region shows the stability of a salt-forming region in the nonequilibrium state, and the so-called isothermal diagram combined the salt-forming diagram with the solubility diagram, giving five one-salt stable regions and a complex conditional region (including eight two-salt regions and four three-salt regions). The conditional region does not exist in the solubility diagram and metastable diagram but occupies a field about 47 % of the diagram's total area where the kind of salt precipitating depends on nonthermodynamic conditions, such as crystal seed, evaporation intensity, mechanical effects, and so forth.

(3) The salt-forming diagram gives more information about solid precipitation and the behaviors of the salt-forming region in the nonequilibrium state, which is extremely valuable to the industry process.

To find out more characteristics of the salt-forming diagram at high temperature and at high evaporation intensity for the complex systems, more experiments are still required; furthermore, thermodynamic and kinetics models are urgently needed.

AUTHOR INFORMATION

Corresponding Author

*Tel.: +8622-60600945; fax: +8622-60600358. E-mail: zhouhuan@tust.edu.cn.

Funding

This work was supported by the National Natural Science Foundation of China (Nos. 20776110, 21176189) and the Nature Science Foundation of Tianjin (No. 11JCZDJC24300).

Notes

The authors declare no competing financial interest.

REFERENCES

(1) Voigt, W. Solubility equilibria in multicomponent oceanic salt systems from t = 0 to 200 °C: Model parameterization and databases. *Pure Appl. Chem.* **2001**, *73* (5), 831−844.

(2) Cohen-Adad, R.; Balarew, C.; Tepavitcharova, S. Sea-water solubility phase diagram, Application to an extractive process [J]. *Pure Appl. Chem.* **2002**, *74* (10), 1811−1821.

(3) Kurnakov, N. S.; Nikolaev, V. I. Proceeding of the sector of physico-chemical analysis. *Izv. Sekt. Fiz. Khim. Anal. IONKh, USSR* **1938**, *10*, 333−336.

(4) Jin, Z. M.; Xiao, X. Z. Studies on the meta stable phase equilibrium of Na^+, K^+, Mg^{2+}//Cl^-, SO_4^{2-}−H_2O quinary system at 298 K. *Acta Chim. Sin.* **1980**, *38* (4), 313−321.

(5) Jin, Z. M.; Zhou, H. N.; Wang, L. S. Studies on the metastable phase equilibrium of Na^+, K^+, Mg^{2+}//Cl^-, SO_4^{2-}−H_2O quinary system at 308 K. *Chem. J. Chin. Univ.* **2001**, *22* (4), 634−638.

(6) Jin, Z. M.; Zhou, H. N.; Wang, L. S. Studies on the metastable phase equilibrium of Na^+, K^+, Mg^{2+} //Cl^-, SO_4^{2-}−H_2O quinary system at 288 K. *Chem. J. Chin. Univ.* **2002**, *23* (4), 690−694.

(7) Sang, S. H.; Yin, H. A.; Xing, W. Z. (Solid plus liquid) metastable equilibria in quaternary system (Li_2SO_4 + K_2SO_4 + $Li_2B_4O_7$ + $K_2B_4O_7$ + H_2O) at T = 288 K. *J. Chem. Thermodyn.* **2006**, *38* (2), 173−178.

(8) Sang, S. H.; Yin, H. A.; Zeng, Y. Study on metastable equilibria in quaternary system Li^+, Na^+//SO_4^{2-}, CO_3^{2-}−H_2O at 288 K. *Acta Chim. Sin.* **2006**, *64* (22), 2247−2253.

(9) Zeng, Y.; Ling, X. F.; Ni, S. J. Study on the metastable equilibria of the salt lake brine system Li_2SO_4 + Na_2SO_4 + K_2SO_4 + $Li_2B_4O_7$ + $Na_2B_4O_7$ + $K_2B_4O_7$ + H_2O at 288 K. *J. Chem. Eng. Data* **2007**, *52* (1), 164−167.

(10) Zeng, Y.; Meng, Z. Y. Metastable Phase Equilibria for the Quaternary System Na^+ + K^+ + CO_3^{2-} + $B_4O_7^{2-}$ + H_2O at 273.15 K. *J. Chem. Eng. Data* **2010**, *55* (4), 1623−1627.

(11) Deng, T. L.; Wang, S. Q.; Sun, B. Metastable phase equilibrium in the aqueous quaternary system (KCl plus K_2SO_4 + $K_2B_4O_7$ + H_2O) at 308.15 K. *J. Chem. Eng. Data* **2008**, *53* (2), 411−414.

(12) Deng, T. L.; Li, D. C. Solid-liquid metastable equilibria in the quaternary system (NaCl-KCl-$CaCl_2$-H_2O) at 288.15 K. *Fluid Phase Equilib.* **2008**, *269* (1−2), 98−103.
(13) Deng, T. L.; Yu, X.; Li, D. C. Metastable Phase Equilibrium in the Aqueous Ternary System K_2SO_4 + $MgSO_4$ + H_2O at (288.15 and 308.15) K. *J. Solution Chem.* **2009**, *38* (1), 27−34.
(14) Tepavitcharova, S.; Balarew, C. Crystallisation Kinetics of NaCl, $MgSO_4$·H_2O, Na_2SO_4·$MgSO_4$·$4H_2O$ and Na_2SO_4 in the system Na^+,Mg^{2+} /Cl^-,SO_4^{2-} //H_2O at 25 °C. *Freiberg. Forschungsh. (Naturwiss.)* **2002**, *E3*, 94.
(15) Tepavitcharova, S.; Balarew, C.; Rull, F. Raman spectroscopic studies of ion association in the Na^+, Mg^{2+}/Cl^-, SO_4^{2-}//H_2O system. *J. Raman Spectrosc.* **2005**, *36* (9), 891−897.
(16) Zhou, H. A method of preparing halite and epsomite with bittern. CN Patent 2,008,100,541,98.6, 2008.
(17) Fang, C. H.; Fang, Y.; Guo, Y. M. An X-ray diffraction study on the structure of the supersaturated $MgSO_4$ solutions. *Acta Chim. Sin.* **2004**, *62* (3), 268−273.
(18) Zhou, H.; Cui, S. G.; Sha, Z. L.; Yuan, J. J. Non-equilibrium behavior of salt-forming in boiling evaporation process for the system of $MgSO_4$-Na_2SO_4-H_2O at 373 K. *Acta Chim. Sin.* **2008**, *66* (12), 1483−1489.
(19) Zhou, H.; Cui, S. G.; Sha, Z. L.; Yuan, J. J. Non-equilibrium behavior of salt-forming in boiling evaporation process for the system of $MgSO_4$-K_2SO_4-H_2O at 348 K. *Chem. J. Chin. Univ.* **2008**, *29* (10), 2049−2054.
(20) Zhou, H.; Chen, Y. D.; Zhang, Q. Y. Non-equilibrium State Salt-forming Phase Diagram, Application to the Utilization of Bittern Resource in high Efficiency. *Chin. J. Chem. Eng.* **2010**, *18* (4), 635−641.
(21) Zhou, H.; Zhang, H. L.; Chen, Y. D. Salt-forming Regions of Na^+, Mg^{2+}//Cl^-, SO_4^{2-}-H_2O System at 348.15 K in the Non-equilibria State of Isothermal Boiling Evaporation. *J. Chem. Eng. Data* **2012**, *57*, 943−951.
(22) Howard, S. *Solubilities of Inorganic and Organic Compounds*; Pergamon Press: New York, 1979.